Application of Electroless Nickel−Boron Films for High-Selectivity Pattern Transfer Processes

David I. Ma, Loretta Shirey, Daniel McCarthy, and Alan Thompson†

Nanoelectronics Processing Facility (Code 6804)

Syed B. Qadri

Materials Science and Technology Division (Code 6372)

Walter J. Dressick, Mu-San Chen, Jeffrey M. Calvert,‡ Ravi Kapur,§ and Susan L. Brandow*

Center for Bio/Molecular Science and Engineering (Code 6950), Naval Research Laboratory, Washington, D.C. 20375

Received March 7, 2002. Revised Manuscript Received August 20, 2002

Electroless Ni exhibits excellent plasma etch resistance and has been successfully employed as a hard etch mask in the fabrication of microelectronic and microelectromechanical components and templates for contact printing and biomedical applications. The use of a catalytic agent to initiate electroless deposition is known to directly affect the microstructure and properties of the deposited metal and thus the etch resistance and potential pattern resolution. We have previously reported the development of tin-free colloidal Pd(II) electroless catalysts, which are suitable for initiating the deposition of patterned EL Ni films for use as plasma etch masks. In this work we examine the effect of the Pd(II) precursor on feature resolution, Ni plating rate, and etch resistance. The etch selectivity of deposited films is determined by real-time endpoint detection using laser reflectometry. Both film morphology and the formation of nickel silicides were found to impact the etch resistance in thin (<20 nm) films. Etch selectivity values exceeding 200:1 were observed for thicker EL Ni films on silicon.

Introduction

Many microelectronics applications, such as IC device and MEMS fabrication, require the transfer of lithographic patterns into an underlying substrate. Typically, this is a two step process in which patterns are first defined in a photoresist coating by exposure to patterned radiation and development, followed by pattern transfer through reactive ion etching (RIE). Photolithography utilizing 248 nm (KrF) deep ultraviolet (DUV) radiation is currently the industry standard, capable of generating features with dimensions to ∼180 nm. A shift to higher-energy optical tools (193 nm, 157 nm) and the use of nonconventional exposure tools (extreme-UV, electron projection, and maskless lithography) are being considered to meet increased pattern resolution requirements.[1] Critical to the development of these processes is the availability of photoresist platforms exhibiting sufficient transparency, depth of focus, and sensitivity for exposure by a given radiation source, as well as suitable etch resistance for pattern transfer. Photoresists must also meet practical guidelines of cost, process latitude, and batch-to-batch stability for implementation in fabrication lines.

A key requirement in the development of advanced photoresist systems is progressive increases in etch resistance as fabrication moves to smaller geometries. This arises from the need to use increasingly thinner photoresist layers in order to maintain sufficient transparency in the UV. Photoresist thickness must also be limited in order to prevent pattern collapse, with a maximum height-to-width feature ratio of ∼4:1 being desired.[2] The use of thin photoresist films, however, presents problems with pinhole formation and film homogeneity. Furthermore, postdevelopment and RIE conditions can lead to changes in photoresist morphology and the development of microfissures which degrade feature quality, a problem which would be expected to increase in significance as photoresist thickness is further reduced.[3] One alternative to polymeric resists is the use of a thin, protective etch layer formed from refractory metals and/or oxides. Suitable films may be derived from elements such as titanium,[4] tungsten,[5]

* Corresponding author. E-mail: sbrandow@cbmse.nrl.navy.mil. Mail: Code 6950, Naval Research Laboratory, Washington, DC 20375.
† U. S. Naval Academy, Box 14715, Annapolis, MD 21412.
‡ Present address: Shipley Company, L.L.C., 455 Forest Street, Marlborough, MA 01752.
§ Present address: Anudeza Group, 26 Church Street, Canton, MA 02021.

(1) *International Technology Roadmap for Semiconductors* (International SEMATECH, Ed.) (http://public.itrs.net).
(2) Klopp, J. M.; Pasini, D.; Byers, J. D.; Willson, C. G.; Frechet, J. M. *Chem. Mater.* **2001**, *13*, 4147.
(3) Naeem, M. D.; Yan, W.; Zhu, J. *J. Electrochem. Soc.* **2001**, *148* (3), G137.

10.1021/cm0202308 This article not subject to U.S. Copyright. Published 2002 by the American Chemical Society
Published on Web 10/15/2002

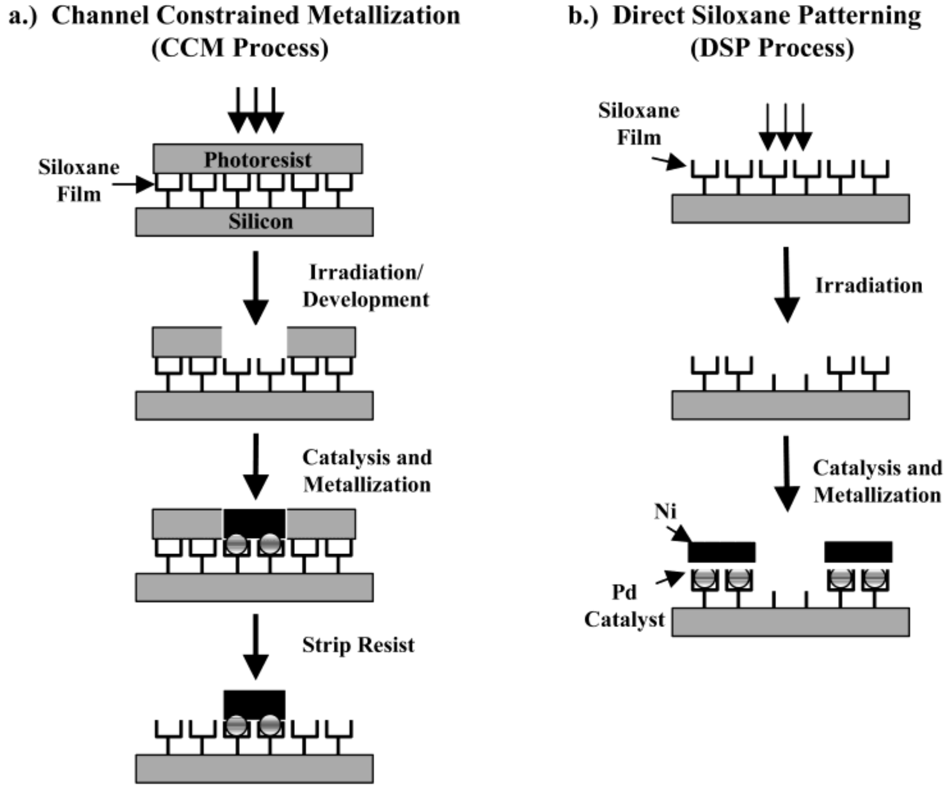

Figure 1. Patterning scheme for the fabrication of EL Ni etch masks by (a) the channel-constrained metallization process (CCM) and (b) direct siloxane film patterning (DSP).

zirconium,[6] and nickel.[7] These materials may be deposited by several deposition techniques, but electroless (EL) deposition is particularly attractive in manufacturing as it allows the low cost metallization of nonplanar, insulating substrates using low-temperature, solution-based chemistries.[8] The resulting films are extremely resistant to RIE and have been successfully used as etch masks in the fabrication of functioning CMOS devices.[7]

We have previously demonstrated two fully additive processes for fabricating EL Ni etch masks using a combination of photolithography and self-assembly. Both approaches utilize a deposited siloxane film containing ligand functional groups, such as phosphines, pyridines, or alkylamines, to chemically bind a Pd species that is used as the EL catalyst. The first method (Figure 1a) is referred to as channel constrained metallization (CCM) and utilizes patterned photoresist to selectively block access to the reactive groups of the siloxane film.[9−11] In this approach a substrate is coated with a ligand siloxane film followed by deposition of a photoresist layer. Exposure and development of the photoresist opens channels to the underlying siloxane film, allowing EL Ni to be selectively deposited in the photoresist channels. The photoresist is then removed leaving the patterned EL metal RIE etchmask. The CCM process is suitable for pattern fabrication as small as $\sim$100 nm while also constraining lateral metal growth which is detrimental to control of feature critical dimensions.

The second process (Figure 1b) is referred to as direct siloxane patterning (DSP). In this approach direct exposure to patterned radiation, which may include DUV, extreme-UV, proximity X-ray, ion-beam, the low-energy electrons of a scanning tunneling microscope (STM), or the electric field of a conducting tip atomic force microscope (AFM), is used to cleave or modify the reactive ligand groups of a siloxane film, creating a pattern of surface chemical reactivity.[12−17] EL Ni is then selectively deposited directly from solution onto the catalyzed intact ligand groups remaining in the unexposed regions of the irradiated film. The DSP process

(4) Katz, H. E.; Schilling, M. L.; Stein, S. M.; Houlihan, F. M.; Hutton, R. S.; Taylor, G. N. *Chem. Mater.* **1995**, *7* (8), 1534.
(5) Stojakovic, G.; Ning, X. J. *J. Vac. Sci. Technol. A* **2000**, *18* (4), 1425.
(6) Schilling, M. L.; Katz, H. E.; Houlihan, F. M.; Kometani, J. M.; Stein, S. M.; Nalamasu, O. *Proc. SPIE* **1994**, *2195*, 182.
(7) Calvert, J. M.; Dulcey, C. S.; Georger, J. H.; Peckerar, M. C.; Schnur, J. M.; Schoen, P. E.; Calabrese, G. S.; Sricharoenchaikit, P. *Solid State Technol.* **1991**, *34* (10), 77.
(8) Mallory, G. O.; Hadju, J. B. *Electroless Plating: Fundamentals and Applications*; American Electroplaters and Surface Finishing Society Press: Orlando, FL, 1990.
(9) Chen, M.-S.; Brandow, S. L.; Dressick, W. J. *Thin Solid Films* **2000**, *379* (1−2), 203.
(10) Chen, M.-S.; Brandow, S. L.; Dulcey, C. S.; Dressick, W. J.; Taylor, G. N.; Bohland, J. F.; Georger, J. H., Jr.; Pavelchek, E. K.; Calvert, J. M. *J. Electrochem. Soc.* **1999**, *146* (4), 1421.
(11) Calabrese, G. S.; Calvert, J. M.; Chen, M.-S.; Dressick, W. J.; Dulcey, C. S.; Georger, J. H.; Bohland, J. (Naval Research Laboratory). Selective Metallization Process. U.S. Patent 5,510,216, 1996.
(12) Dressick, W. J.; Dulcey, C. S.; Georger, J. H.; Calvert, J. M. *Chem. Mater.* **1993**, *5* (2), 148.
(13) Calvert, J. M.; Koloski, T. S.; Dulcey, C. S.; Dressick, W. J.; Peckerar, M. C.; Cerrina, F.; Taylor, J.; Suh, D.; Wood, O.; MacDowell, A. A.; D'Souza, R. *Opt. Eng.* **1993**, *32* (10), 2437.
(14) Perkins, F. K.; Dobisz, E. A.; Brandow, S. L.; Calvert, J. M.; Kosakowski, J. E.; Marrian, C. R. K. *Appl. Phys. Lett.* **1996**, *68* (4), 550.
(15) Brandow, S. L.; Snow, E. S.; Campbell, P. M.; Calvert, J. M. *J. Vac. Sci. Technol. A* **1997**, *15* (3), 1455.
(16) Dressick, W. J.; Dulcey, C. S.; Brandow, S. L.; Witschi, H.; Nealey, P. F. *J. Vac. Sci. Technol. A* **1999**, *17* (4), 1432.
(17) Ada, E. T.; Hanley, L.; Etchin, S.; Melngailis, J.; Dressick, W. J.; Chen, M.-S.; Calvert, J. M. *J. Vac. Sci. Technol. B* **1995**, *13* (6), 2189.

is suitable for pattern fabrication significantly below 100-nm dimensions; however, attention must be paid to limiting the EL Ni mask thickness to control lateral Ni growth.

The materials properties, and hence the etch resistance, of deposited EL metal films are known to be directly correlated to deposition conditions and film structure.[18] Furthermore, it is well-known that the use of catalytic agents to initiate electroless deposition on insulating surfaces dramatically affects both the microstructure and properties of deposited metal films.[19−25] We utilize a new class of Pd(II) based colloids as catalysts for selective electroless metal deposition on siloxane templates.[25−27] In this work we examine preparation conditions affecting the particle size and catalytic activity of Pd(II) colloidal dispersions. We also investigate the film deposition rates, microstructure, and etch resistance of EL Ni−boron films deposited from colloidal Pd(II) catalytic precursors on CCM patterned samples. Etch selectivities of Ni over Si as high as ∼200:1 for thick (i.e., >35 nm) NiB films fabricated by the CCM process were observed with good lateral confinement, indicating that the etch masks are suitable for the fabrication of high-aspect-ratio features with significant relief. The determination of nickel−silicide formation at the interface during plating, as well as the morphology of the deposited catalyst and EL Ni layers is discussed as it relates to meeting process latitude requirements for the etching of high-resolution DSP patterned samples.

Experimental Section

Reagents. Deionized (DI) water of 18 MΩ resistivity was used for all experiments. All reagents were ACS reagent grade or better and were used as received unless otherwise noted. The organosilane N-(aminoethyl)-3-aminopropyltrimethoxysilane (EDA) was obtained from Gelest, Inc., purified prior to use by vacuum distillation (140 °C, 14 mmHg), and stored under dry nitrogen atmosphere until needed. The organosilane (aminoethylaminomethyl)-phenethyltrimethoxy silane (PEDA) was obtained from Gelest, Inc. and used as received. Semiconductor grade NaOH (99.99%), morpholinoethane sulfonic acid, and Na_2PdCl_4 (99%) from Aldrich were used for preparation of the EL catalysts. Substrates were p-type Si(100) (VA Semiconductor) doped to 10−20 Ω cm. S1400-27 photoresist and MF312 developer (0.27 N) were obtained from Shipley Co. The electroless Ni bath NIPOSIT 468 (pH 7, Shipley Co.) was prepared according to manufacturer's instructions and diluted to 10% strength with DI water prior to use.

Siloxane Film Formation. Silicon wafers were cleaned by successive immersions in HCl/CH_3OH (1:1 v/v), DI water (triple rinse), and concentrated H_2SO_4, and then stored in gently boiling water until needed for film formation.[28] Films of the EDA[10] and PEDA[9,29] organosilanes were prepared by dip coating using literature methods. Upon removal from the treatment solutions the wafers were rinsed with methanol and dried under a stream of filtered nitrogen. Films of the EDA organosilane were also prepared by spin coating. Briefly, a 1% w/v aqueous EDA organosilane solution containing 1 mM acetic acid as a film deposition catalyst was puddled onto a Si wafer mounted on the vacuum chuck of a spin coater. Following a deposition time of 1 min, the wafer was spun at 3 krpm for 15 s under a stream of DI water, and then spun dry for an additional 15 s. Wafers prepared by both methods were baked on a programmable hotplate at 120 °C for 3−4 min to complete the dehydration reaction that forms the siloxane bond between the organosilane and the substrate. Measurements of film thickness (Gaertner model 115C ellipsometer) and advancing water contact angle (Zisman-type contact angle apparatus) were used to monitor film quality.[30] EDA films prepared by solution deposition and spin coating exhibit similar siloxane film thicknesses, film homogeneity, and reactivity toward the binding of Pd catalysts.[10]

Pattern Formation. *Channel Constrained Metallization (CCM) Process.* All steps in the CCM patterning process were performed in a class 1000 clean room under yellow safe lights. Planarizer films were fabricated by spin-coating Shipley Co. S1400-26 photoresist for 30 s at 5 krpm to produce 1.10-μm thick films, followed by thermal cross-linking at 210 °C for 10 min using a Wentworth Labs model TC-100 vacuum hotplate (Wentworth Laboratories, Inc.). The resulting films retained a sufficient concentration of surface hydroxyl groups to permit chemisorption of the EDA organosilane. EDA coated planarizer or silicon wafers were spin coated with Shipley S1400-27 photoresist at 4 krpm for 30 s to form a uniform coating approximately 1.3 μm thick.[10] Photoresist films were subjected to a postapplication bake in a Grieve model LW-201C oven (Grieve Corp.) at 90 °C for 30 min. The substrate was patterned by placing a chrome-on-quartz mask in direct contact with the photoresist layer and irradiating with a broad band Hg lamp contact aligner (Karl Suss, 365−405 nm output) to a dose of 150 mJ/cm^2. Development with Shipley developer MF312 (0.27 N) for 120 s was used to remove the exposed photoresist, and was followed by a DI water rinse.

Direct Siloxane Patterning (DSP) Process. The EDA siloxane film was directly patterned by exposure to pulsed deep UV ArF excimer laser light (Questek 2430) through a chromium mask to produce a patterned array of siloxane and deep UV cleared areas. Typically the uniform central portion of the excimer output was apertured, enlarged with a negative focal length fused silica lens, and directed onto a 4 cm^2 area of the mask/wafer assembly. Irradiation of the EDA films at 193 nm under ambient conditions at exposure doses of 30 J/cm^2 is sufficient to remove the amine-containing functional group and prevent catalyst binding and metallization.[31] The PEDA siloxane film was directly patterned by exposure to the low-energy electrons of a scanning tunneling microscope as described elsewhere.[14]

Catalysis and Metallization. Following patterning, substrates were treated with either of two colloidal Pd(II) catalyst formulations (PD1 or PD2). Catalyst dispersion PD1 was prepared according to the literature method and stored in a

(18) Hintermann, H. E. *Schweizer Arch.* **1969**, *35*, 217.
(19) Feldstein, N.; Schlesinger, M.; Hedgecock, N. E.; Chow, S. L. *J. Electrochem. Soc.* **1974**, *121* (6), 738.
(20) Cortijo, R. O.; Schlesinger, M. *J. Electrochem. Soc.* **1983**, *130* (12), 2341.
(21) Cortijo, R. O.; Schlesinger, M. *J. Electrochem. Soc.* **1984**, *131* (12), 2800.
(22) Horkans, J.; Kim, J.; McGrath, C.; Romankiw, L. T. *J. Electrochem. Soc.* **1987**, *134* (2), 300.
(23) O'Sullivan, E. J. M.; Horkans, J.; White, J. R.; Roldan, J. M. *IBM J. Res. Dev.* **1988**, *32* (5), 591.
(24) Homma, T.; Tanabe, M.; Itakura, K.; Osaka, T. *J. Electrochem. Soc.* **1997**, *144* (12), 4123.
(25) Brandow, S. L.; Dressick, W. J.; Marrian, C. R. K.; Chow, G.-M.; Calvert, J. M. *J. Electrochem. Soc.* **1995**, *142* (7), 2233.
(26) Brandow, S. L.; Chen, M.-S.; Wang, T.; Dulcey, C. S.; Calvert, J. M.; Bohland, J. F.; Calabrese, G. S.; Dressick, W. J. *J. Electrochem. Soc.* **1997**, *144* (10), 3425.
(27) Dressick, W. J.; Kondracki, L.; Chen, M.-S.; Brandow, S. L.; Matijevic, E.; Calvert, J. M. *Colloids Surf. A* **1996**, *108* (1), 101.
(28) Dressick, W. J.; Dulcey, C. S.; Georger, J. H.; Calabrese, G. S.; Calvert, J. M. *J. Electrochem. Soc.* **1994**, *141* (1), 210.
(29) Dressick, W. J.; Dulcey, C. S.; Chen, M.-S.; Calvert, J. M. *Thin Solid Films* **1996**, *285*, 568.
(30) Arkles, B. In *1992 Huls Silicon Compounds Register and Review;* Anderson, R., Larson, G. L., Smith, C., Eds.; Huls America Inc.: Piscataway, NJ, 1992; p 59. Siloxane film thickness was determined by first measuring the optical constants for the wafer and assuming that the refractive index of the film is given by the manufacturer's value for the index of refraction [η_D(EDA) = 1.442 and η_D(PEDA) = 1.5083].
(31) Stenger, D. A.; Georger, J. H.; Dulcey, C. S.; Hickman, J. J.; Rudolph, A. S.; Nielsen, T. B.; McCort, S. M.; Calvert, J. M. *J. Am. Chem. Soc.* **1992**, *114*, 8435.

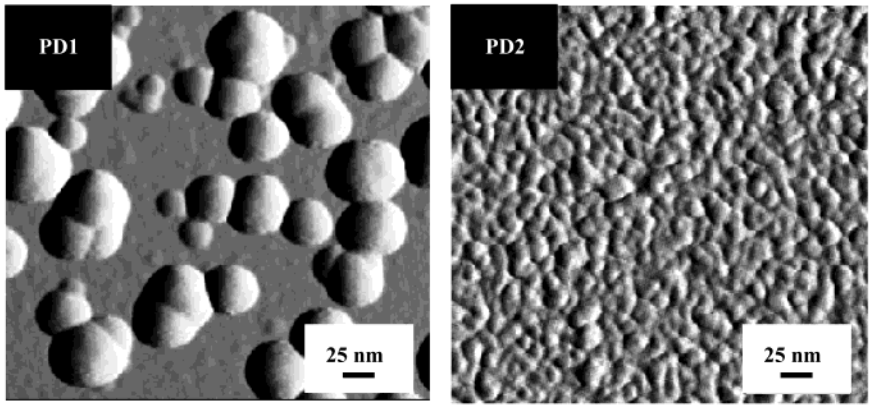

Figure 2. Tapping mode AFM images of siloxane coated silicon surfaces treated with the PD1 catalyst for 30 min or the PD2 catalyst for 2 min.

water bath at 22 °C until used.[25,27] Catalyst dispersion PD2 was prepared according to an alternate literature method followed by dilution with 1 M NaCl to 75% strength for use with DSP patterned samples or dilution to 50% strength for use with CCM patterned samples.[26] The PD2 dispersion was filtered through a 0.2-μm Teflon filter and used immediately. Samples were catalyzed for 30 min with PD1 or 3 min with PD2. Following catalysis, samples were rinsed gently with DI water and immersed in Shipley 468 Ni bath (10% strength, 22 °C) for times ranging from 1 to 120 min to produce samples with various Ni film thicknesses. Metallized CCM substrates were stripped of the residual unexposed S1400-27 photoresist by spraying the wafer with a stream of acetone for ~10 s, followed by rinsing with DI water and drying under filtered nitrogen. In experiments studying the thickness of catalyzed surfaces following treatment with a reducing agent, catalyzed samples were immersed in a solution of dimethylamine borane (DMAB) (0.5 g/100 mL of DI water) for 4 min. Surfaces were then rinsed with DI water and blown dry with filtered nitrogen.

Reactive Ion Etching. Patterned samples were etched in a Plasmatherm 500 series reactive ion etching system using 16 sccm of SF_6 and 12 sccm of CHF_3 at a total pressure of 20 mTorr. The etching conditions for all samples were held constant except for etch time. The total radio frequency (RF) power was adjusted to maintain a sample bias voltage of 100 V while keeping the electrode at room temperature (22 °C), and etching time was broken down into intervals of 30-min etches followed by 30-min pumpdowns. The RIE system was equipped with a laser endpoint detection apparatus, employing a 2 mW HeNe laser positioned 90° relative to the sample surface. The laser spot measured 1 mm in diameter and was fixed in relation to the sample position. Following SEM evaluation the Ni film was stripped from samples by rinsing them in dilute nitric acid.

Sample Characterization. Substrate images were obtained at various process stages using a Leica 360 Field Emitter scanning electron microscope (SEM). Atomic force microscope (AFM) images were obtained using a Nanoscope III AFM (Digital Instruments) equipped with microfabricated silicon cantilevers with a bending modulus of approximately 30−50 N/m. Images were acquired in tapping mode and data processing consisted of a correction to account for sample tilt followed by the application of a median filter. Feature height measurements were also obtained using a Tencor P-2 profilometer equipped with a 0.5-μm probe tip. X-ray diffraction (XRD) spectra of the deposited EL Ni films were obtained on a Rigaku diffractometer using $CuK_{\sigma 1}$ radiation (0.154178 nm) with a sweep time of one minute per degree.

Results and Discussion

Catalyst Development. The use of EL Ni films as etch masks in high-resolution applications requires the development of small, monodisperse colloidal catalysts to maintain critical dimension control of plated features. Modern colloid theory predicts that particle size will be controlled by the relative rates of nucleation of new particles and the growth of existing particles during catalyst formulation or ripening,[32] as demonstrated by the formation of the PD1 and PD2 catalyst dispersions. Briefly, each catalyst is formed by the controlled hydrolysis of the $PdCl_4^{2-}$ species in aqueous solution.[33] Hydrolysis of the coordinated chloride ligands, in combination with deprotonation of the resulting mixed chloro−aquo complexes, leads to the formation of reactive hydroxy−Pd(II) species. Irreversible condensation of these species leads to the formation of μ-hydroxy and/or μ -chloro-bridged Pd(II) oligomers, which function as nuclei for colloid formation. For example, formation of PD1 entails slow hydrolysis (i.e., Ostwald ripening) of $PdCl_4^{2-}$ in pH 5 aqueous solution containing ~10 mM added NaCl. Because the ripening process for PD1 is slow under these conditions, colloid nucleation and growth compete. The resulting particles have a large average size (~31 ± 13 nm) and wide size range (~4−53 nm). This can be seen in the AFM image of a PD1 catalyzed surface (Figure 2).[26]

Although the PD1 catalyst has been used successfully to metallize CCM features as small as 100 nm, the feature critical dimension control and fidelity of pattern replication during metallization of sub-200-nm DSP features is clearly limited by the presence of larger catalyst particles in the PD1 distribution. Metallization of surfaces treated with PD1 yields metal films composed of metal particles exhibiting maximum diameters in excess of 100 nm.[25,27] In the absence of the CCM photoresist sidewall to constrain catalyst binding and metallization, the larger catalyst particles and subsequently deposited EL metal in DSP patterns can inadvertently “bridge” adjacent small features, compromising replication of the surface template. Increased edge roughness in metallized features results in a “grainy” appearance, which has been previously observed in 150-nm DSP features patterned by proximity X-ray,[34] while the bridging of adjacent features due to metal overgrowth is observed in smaller 30-nm metal-

(32) Ross, S.; Morrison, I. D. In *Colloidal Systems and Interfaces*; John Wiley & Sons: New York, 1988.
(33) Rund, J. V. *Inorg. Chem.* **1970**, *9*, 1211.
(34) Yang, X. M.; Peters, R. D.; Kim, T. K.; Nealey, P. F.; Brandow, S. L.; Chen, M.-S.; Shirey, L. M.; Dressick, W. J. *Langmuir* **2001**, *17* (1), 228.

lized DSP features patterned by scanning tunneling microscope (STM) lithography.[35]

Metallization of sub-100-nm features requires the use of near monodisperse catalyst dispersions having an average particle size smaller than the feature width to avoid "bridging" problems. Such catalysts can be prepared under conditions where nucleation dominates growth during the ripening process. For $PdCl_4^{2-}$ based catalysts, nucleation can be enhanced by a sudden increase in pH at the start of the ripening process. Large amounts of aquochloro- and hydroxychloropalladium (II) species are rapidly formed in solution and condense to form large numbers of similarly sized nuclei. Because this process depletes the solution of the $PdCl_4^{2-}$ raw material needed for particle growth, subsequent growth is inhibited. This results in a significant reduction in the polydispersity and average size of the colloid distribution. Preparations carried out in this manner produce catalysts such as PD2, which exhibits an average particle size of 9 ± 3 nm and a particle size range of ∼< 4−18 nm, as shown in the AFM image of Figure 2 (PD2). Metallization of surfaces treated with PD2 yields metal films with an average metal particle size of 21 ± 5 nm.[26] These improvements in catalyst size and monodispersity have been shown sufficient to successfully metallize ∼15-nm STM patterned features with good edge resolution and line-width control.[14] Thus, replacement of the PD1 catalyst with the PD2 formulation during processing results in markedly improved feature fidelity at high resolutions.

We attempted to further reduce the size and polydispersity of the $PdCl_4^{2-}$ based catalysts by varying the following conditions during colloid growth: (1) solution basicity during ripening; (2) solution ripening time; (3) the fraction of base neutralized after ripening; and (4) the [NaCl] in solution during ripening. Using the PD2 formulation as a starting point, we prepared additional catalysts dispersions by varying the level of NaOH added to initiate ripening from 0.05 M to 0.20 M, the level of [NaCl] during ripening over the range 0.4 to 4.0 mM, and the ripening time from 2 to 4 h. An HCl solution of molarity equal to that of the base solution (complete neutralization) or an HCl solution whose concentration was sufficient to neutralize 90% of the added base solution (incomplete neutralization) was used to quench the ripening process. Catalyst solutions were tested immediately after quenching by applying the catalyst dispersion to an EDA substrate for 2 min followed by standard aqueous rinsing and metallization.

Samples were evaluated based upon AFM imaging of the metallized substrates. The Ni−B EL plating bath used in these experiments has a grain size of less than 7 nm and therefore did not significantly affect film morphology.[36] As expected, variation of the catalyst parameters did significantly influence the particle size of the deposited Ni metal. The experiments confirm that, in general, as ripening time decreases, there is a tendency toward formation of smaller Ni particles. There is also an indication that the addition of larger quantities of HCl during the quenching process and the presence of larger amounts of NaCl during ripening

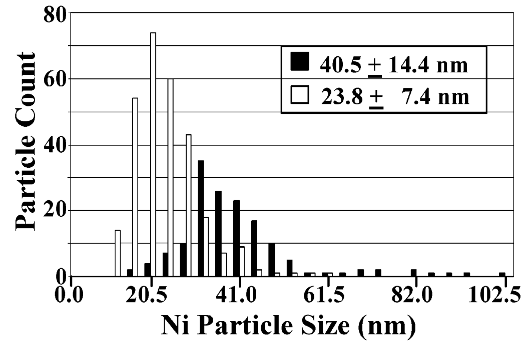

Figure 3. Ni particle distributions for the alternative catalyst formulations yielding the smallest (23.8 ± 7.4 nm) and largest (40.5 ± 14.4 nm) Ni particle sizes. Observations are consistent with the proposed hydrolysis model.

contributes ultimately to smaller Ni particle formation. These observations are consistent with our hydrolysis model[26−28] and show that it is possible to rationally control the Ni particle size through changes in the catalyst solution variables. The AFM images and Ni particle distribution histograms for the two formulations in the study yielding the largest Ni particles (∼40.5 ± 14.4 nm) and the smallest Ni particles (∼23.8 ± 7.4 nm) are shown in Figure 3 for comparison.[37] Unfortunately, none of the formulations tested yielded smaller or less polydisperse particles than those previously obtained using PD2. Therefore, we used the PD1 and PD2 catalyst formulations for the remainder of our experiments to evaluate plating and etch resistance of the deposited EL Ni films.

EL Ni Plating Rates and Metal Etch Resistance. Evaluation of EL plating rates and metal etch resistance was performed on samples containing micron-size patterns fabricated using the CCM process.[38] Samples were catalyzed with either PD1 or PD2 and plated for times ranging from 1 to 120 min. Following stripping of the residual photoresist, the EL Ni/Pd layer thickness was measured by profilometery and AFM. Profilometry systematically yielded slightly higher thickness readings than those obtained by AFM, however, measurements typically agreed within 10%. To determine the thickness of the deposited EL Ni, especially for the shorter Ni deposition times, the thickness of the underlying Pd catalyst must be subtracted from the measured EL Ni/Pd layer thickness.[39] The catalyst layer thickness was determined by AFM imaging of catalyzed DSP line/space patterns. Although the catalysts are deposited as

(35) Marrian, C. R. K.; Perkins, F. K.; Brandow, S. L.; Koloski, T. S.; Dobisz, E. A.; Calvert, J. M. *Appl. Phys. Lett.* **1994**, *64* (3), 390.

(36) Data sheet for NIPOSIT 468 Ni−B bath (Shipley Co.).

(37) Catalyst formulation A (Ni particle diameter ∼ 23 nm) was prepared using 0.05 M [NaOH], 0.4 mM [NaCl], 2 h ripening time, and complete neutralization of base to quench colloid growth. Catalyst formulation B (Ni particle diameter ∼ 43 nm) was prepared using 0.20 M [NaOH], 0.4 mM [NaCl], 4 h ripening time, and incomplete neutralization of base at quenching. Several of the catalyst preparations were found inactive immediately following preparation. Catalytic inactivity was accompanied by bulk precipitate formation and/or a failure to bind catalyst (as exhibited by a lack of surface wetting) on the substrate surface.

(38) The CCM process requires complete clearing of the resist in order to expose the ligating sites of the siloxane film. Incomplete clearing can result in lower surface coverages of catalyst and changes in the plating rate. To rule out any discrepancy in the data due to photoresist residue in the channels, a series of metal patterns were prepared both by direct DUV photopatterning of siloxane films (DSP process) as well as by the CCM process. Metal thickness measurements for both sets of samples are in good agreement (within 10%), indicating that any residual photoresist on CCM samples does not significantly alter EL Ni deposition rates.

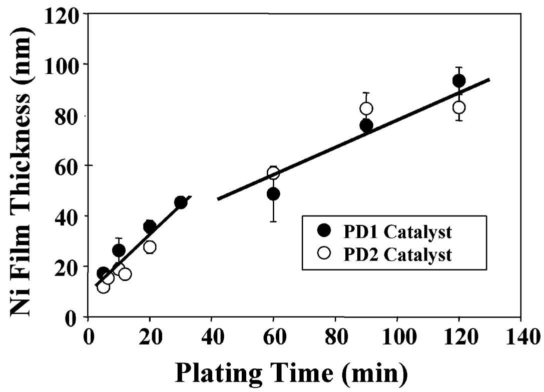

Figure 4. EL Ni deposition rates on PD1 and PD2 catalyzed surfaces as measured by profilometer and corrected to account for the thickness of the underlying catalyst.

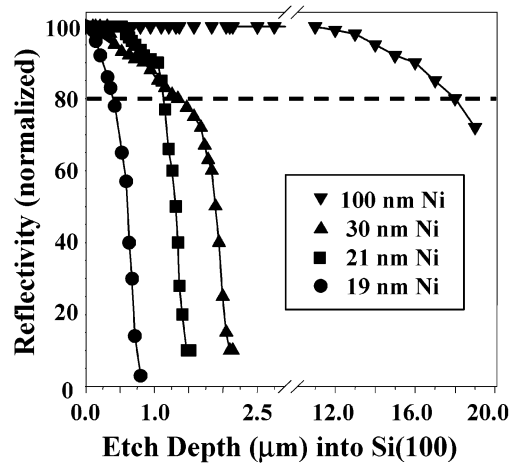

Figure 5. Reflectivity signal plotted as a function of Si etch depth for EL Ni masking layers of various thicknesses. The dashed line marks the point at which the reflectivity signal has dropped by 20%.

Pd(II) species, the bound Pd(II) is exposed to a reducing agent in the plating bath, reducing it to Pd(0), which actually functions as the catalytic species. Therefore the catalyzed Pd(II) surfaces were treated with an aqueous solution of the reducing agent dimethylamine borane prior to imaging. This treatment results in reduction of the Pd(II) to the zerovalent form, with a 20% loss of Pd from the surface.[28] The catalyzed and reduced surfaces yielded reduced PD1 and PD2 layer thicknesses of 15.1 $\pm$ 4.5 nm and 7.0 $\pm$ 3.2 nm, respectively. The resulting EL Ni film thickness on PD1 and PD2 catalyzed surfaces is plotted as a function of plating time in Figure 4. For deposition times less than 30 min the plating on both reduced PD1 and PD2 surfaces occurs at a linear rate of approximately 1.2 nm/min. This growth region, corresponding to the deposition of Ni directly onto the Pd(0) sites, indicates that the catalytic activity of the Pd(0) generated by the PD1 and PD2 surfaces is comparable. After approximately 30 min the EL Ni deposition transitions to a slower rate of approximately 0.6 nm/min as the Pd(0) sites become covered with the NiB film and plating becomes autocatalytic.

To evaluate the etch resistance of the deposited Ni films, wafers were cleaved in half to provide one sample for depth and etch rate measurements and a second sample for reflectivity measurements. Depth and etch rate measurements were conducted by periodically removing the sample from the etching chamber and measuring the etch profile by SEM and profilometry. Cross-sections of the surface were also viewed by SEM to determine the sidewall profile, the overall uniformity of Si etching, the extent of Ni mask breakthrough, and sample surface roughness. Reflectivity measurements to monitor Ni coverage were conducted by reflecting a laser from the sample surface and recording the laser signal in real time during RIE. Changes in the reflectivity signal were correlated with SEM evaluation of the Ni masking layer integrity and etch depth for Ni layers of various thicknesses (Figure 5). Good mask integrity was retained for reflectivity values $\geq$ 80% of initial value. In this regime good agreement was obtained between SEM and profilometry measurements, and etched features exhibited good definition and edge acuity (Figure 6a).

Samples were also evaluated for evidence of nonuniform etching due to etch mask breakthrough. During an extended RIE, plasma erosion results in a gradual thinning of the metal etch mask. As the Ni film is eroded its morphology is ultimately dominated by the underlying catalyst particles and the substrate surface. Mask failure most likely begins with breakthrough of the plasma in the weak intergranular regions of the thinner Ni mask, where etch rates are enhanced.[3] Differential etch rates between the Ni mask and the exposed Si substrate (Figure 7, vide infra) in these breakthrough regions promotes nonuniform etching in the area of the sample originally completely covered by the Ni etch mask. This difference in etch rates leads to a roughening of the surface and the formation of jagged needlelike metal protected structures in the NiB masked areas, as shown in Figure 6b. That is, the etch selectivity is effectively destroyed because of this surface “micromasking” by the remaining intact Ni/Pd particles of the mask once breakthrough occurs. As etching continues, sputtering and redeposition of Pd/Ni particles from the Ni mask onto the unmetallized regions of the sample eventually occurs, leading to micromasking of these regions as well and further degradation of the etch quality (not shown). The increased roughness and micromasking associated with breakthrough contribute to erroneous profilometry results at these longer etch times. Therefore, SEM measurements were used exclusively to determine etch depths for samples exhibiting reflectivities <80%. These behaviors clearly contrast with those in Figure 6a, in which the high and uniform reflectivity of the Ni masked regions of the substrate indicate the presence of a Ni film of sufficient homogeneity and thickness to protect the underlying substrate during RIE.

The etch selectivity of Si over Ni during RIE is due to rate differences in the chemical reactions taking place at the surface of these materials as well as ion bombardment, with the surface fluorination of silicon lead-

(39) The composite thickness of the catalyst/EL Ni layers depends on the thickness of the initial catalyst layer, which is different for PD1 and PD2. To determine the catalyst layer thicknesses DSP 5 micron line/space patterns were catalyzed with either PD1 or PD2, reduced to the catalytic Pd(0) species, and imaged by AFM. The height of the catalyst layers was then subtracted from the measured height of the Pd/Ni layer, allowing EL Ni thicknesses to be directly compared. The surface bound Pd(0) particles were found to have no appreciable plasma etch resistance in the absence of a deposited EL Ni layer.

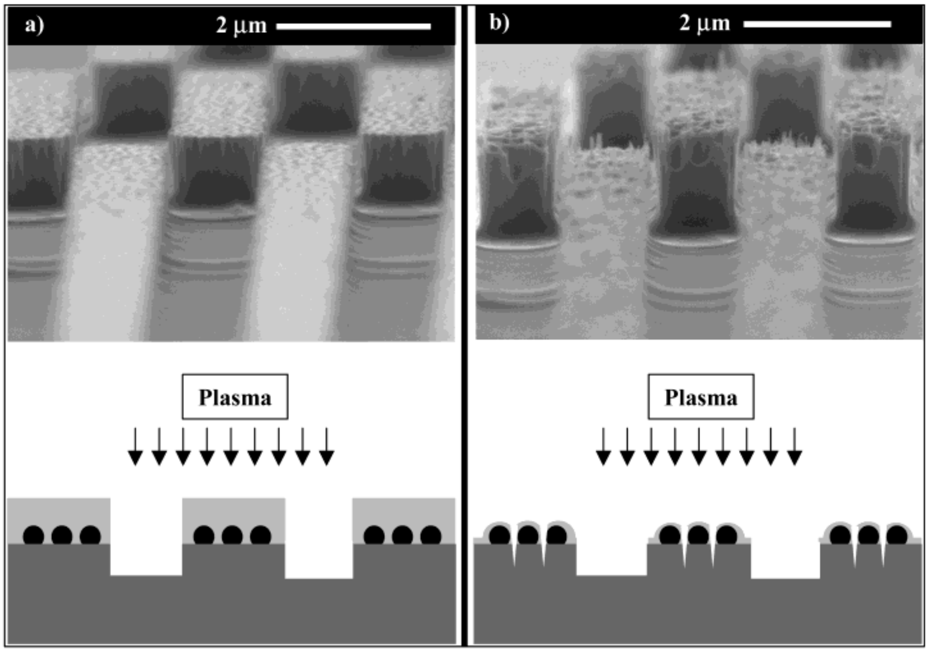

Figure 6. SEM micrographs showing reactive ion etching results for a 30 nm thick NiB etch mask. NiB patterned Si wafers are cleaved and viewed edge on to highlight the etch selectivity and quality. RIE conditions are given in the Experimental Section. (a) NiB (bright areas) masked Si substrate after etching to a depth of ~1.0 μm. Note the high reflectivity (i.e., ~90%, Figure 5) of the Ni regions, the sharp edges and vertical sidewalls of the features, and the smooth floors of the unmetallized, etched Si regions. (b) Same region shown in part (a) after etching to a depth of 1.6 μm showing the onset of NiB mask breakthrough. Note the decreased reflectivity (i.e., ~75%, Figure 5) and presence of needlelike structures resulting from breakthrough and metal particle micromasking in the NiB regions, as well as the degradation in the feature sidewall profiles as etching becomes less uniform. The uniformity of the etched Si channel floors in the unmetallized regions confirms that micromasking due to sputtering and redeposition of metal particles from the Ni mask onto these regions is not yet an appreciable problem at this stage of RIE.

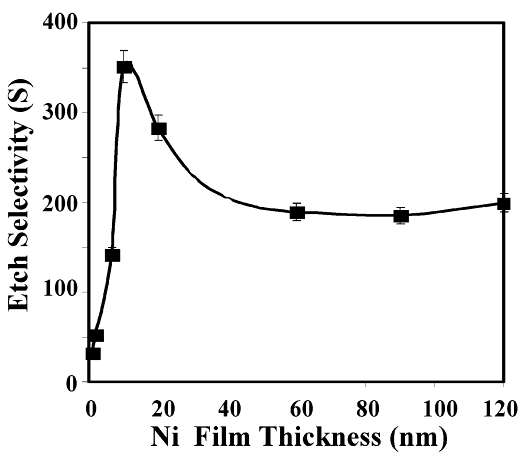

Figure 7. Etch selectivity (S), as defined in eq 1, plotted as a function of EL Ni film thickness. A 20% drop in the surface reflectivity of Ni was used to determine the etching endpoint.

ing to the production of SiF_4 which desorbs from the surface as a gas.[40] For the purpose of this work the etch selectivity ratio is defined as follows:

$$\text{Etch Selectivity} = S = T_{\mathrm{Si}}/T_{\mathrm{Ni}} \qquad (1)$$

where T_{Si} = Si etch depth at 80% reflectivity and T_{Ni} = original plated thickness of the EL Ni film.

(40) Economou, D. J. The Chemistry of Plasma Etching. In *Electronic Materials Chemistry*; Pogge, H. B., Ed.; Marcel Dekker: New York, 1996; pp 251−322.

A plot of the etch selectivity as a function of EL Ni thickness is shown in Figure 7. The intrinsic etch selectivity of the EL Ni film increases with Ni layer thickness, eventually stabilizing at a value of approximately 200:1 for Ni films of thickness greater than 50 nm. The reduced etch selectivity for thinner masking layers (<15 nm) is likely attributable to the morphology of the film, which is dominated by the granular appearance of the underlying catalyst.[26] Similar to the mechanism shown in Figure 6b, mask failure likely begins with breakthrough in the intergranular regions of thin EL Ni films. Of particular interest is a peak in the etch selectivity at a Ni thickness of 15 nm, where the etch resistance reaches a value of ~350:1. To investigate the nature of this effect Ni films of thicknesses 7, 20, 45, and 165 nm were examined by X-ray diffraction. The XRD spectra of the EL Ni films are shown in Figure 8. The deposited EL Ni film exhibits a face centered cubic (fcc) structure in these samples. The dominant (111) and (200) peaks of fcc nickel with relative intensity of 1 at 44.5° and 0.4 at 51.8° are clearly observed, as well as the secondary (220) and (311) peaks with intensities of 0.2 at 76.4° and 92.9° in the two thicker samples. There are also two additional minor peaks at 65° and 75°, which appear to dominate the initial plating stage. These peaks are attributable to the formation of mixed peaks of nickel silicide, most likely (Ni_3Si) and (Ni_2Si).[41] The formation of nickel-silicides at the interface of

(41) Nicolet, M.-A.; Lau, S. S. Formation and Characterization of Transition-Metal Silicides. In *VLSI Electronics: Microstructure Science, Vol. 6*; Einspruch, N. G., Larrabee, G. B., Eds.; Academic Press: New York, 1983.

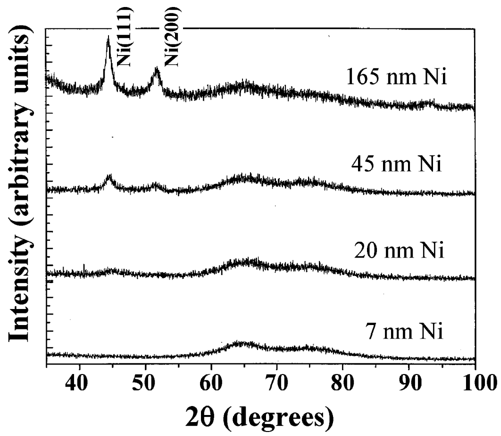

Figure 8. X-ray diffraction spectra of EL Ni films of various thicknesses. The main diffraction peaks observed are associated with diffraction from the planes (111), (200), (220), and (311) of face centered cubic Ni. Two minor peaks at 65° and 75° are associated with the formation of nickel silicides.

silicon and nickel surfaces under room-temperature conditions and their excellent etch resistance is well documented.[42−44] The fact that the increase in etch resistance is gradual, peaking approximately 10 to 15 min into the EL Ni deposition, may be attributable to the presence of the Pd catalyst. The presence of a Pd interlayer has previously been shown to act as a diffusion barrier significantly slowing the formation of silicides.[45] Under our plating conditions the EL Ni and silicon substrate are separated by an nonuniform colloidal Pd layer (Figure 2). This likely leads to varied rates of localized silicide formation and contributes to the variations in etch rates observed in thin EL Ni films. As plating continues the silicide is gradually buried under EL Ni and the etch resistance of the film is dominated by the properties of the deposited EL Ni film.[46]

Etched patterns fabricated by the CCM process using standard contact deep-UV photolithography on planarizer and silicon substrates are shown in Figure 9a and b, respectively. The Ni etch mask was left intact to minimize charging during SEM imaging. From the images it is evident that this process can be used to produce features with good sidewall control and reproducibility with no evidence of micromasking. A 100-nm thick Ni film provides sufficient etch resistance for pattern transfer to approximately 19 μm, as shown in Figure 9c. Thicker films, up to several microns thick prepared using the CCM process, can be used to fabricate masks for deep etching applications such as MEMS.

The formation of high resolution (<100 nm) patterned Ni etch masks can be accomplished using direct photopatterning of siloxane films in combination with fine grained Pd(II) catalysts such as PD2. Because of the isotropic growth of Ni during EL Ni deposition, it is particularly important to use extremely thin Ni etch masks for the patterning of sub-100-nm features using the DSP approach. Although mask breakthrough and micromasking must be monitored, we have shown that Ni masks as thin as 7.5 nm are sufficient for RIE pattern transfer to depths of 200 nm with good pattern fidelity.[47]

An example is shown in Figure 9d, where metallized DSP patterns ranging in size from ∼15 to 24 nm in width have been patterned by STM lithography of a PEDA film.[14] STM exposure leads to destruction of the ligating functionality of the siloxane film in a highly localized and controlled manner. Catalysis of the siloxane template with the PD2 catalyst was followed by EL Ni metallization and etching to a depth of approximately 100 nm. The resulting high-resolution patterns exhibit good edge acuity and no evidence of bridging or Ni overgrowth. Analysis of measurements from high-resolution SEM micrographs yields a standard deviation of less than 4 nm in the line width and a line edge roughness of ∼2.7 nm.

Conclusion

In this study we have investigated the film deposition rates, microstructure, and etch resistance of EL Ni−B films. Catalytic colloidal Pd(II) precursors, bound to patterned siloxane films, were used to selectively activate the surface for metal deposition. Although both the PD1 and PD2 catalysts were found to exhibit equivalent EL plating activity, the PD2 catalyst's smaller particle size and narrower particle size distribution is more suitable for high resolution (<100 nm) feature fabrication. Deposited EL Ni films exhibited excellent etch resistance. Whereas thinner EL Ni films are essential for high-resolution pattern transfer processes and are adequate for pattern transfer in integrated circuit fabrication, mask breakthrough must be closely monitored. Surface reflectivity measurements were found to be an effective technique for real-time assessment of etch mask damage. The morphology of thinner EL Ni films (<15 nm), both thinly deposited films and films which have undergone significant Ni removal through the etch process, is dominated by the presence of the underlying catalyst. The interfacial Ni/Pd region (∼5−15 nm thick) consists mainly of Pd(0) particles bridged by deposited metal. The Pd(0) particles offer little etch resistance, and etch breakthrough in the intergranular regions of this layer can lead to mask failure, sputtering of material, and micromasking. Thicker deposited EL Ni films exhibit etch selectivities exceeding 200:1 compared to silicon for Ni film thickness $\geq$ 20 nm, with demonstrated pattern transfer to a depth of ∼19 μm. A peak in the etch resistance at Ni layer thicknesses of ∼15 nm is attributable to the formation of nickel silicides.

(42) Rastegaeva, M. G.; Andreev, A. N.; Zelenin, V. V.; Babanin, A. I.; Nikitina, I. P.; Chelnokov, V. E.; Rastegaev, V. P. *Inst. Phys. Conf. Ser.* **1996**, *142*, 581.

(43) Choi, N. I.; Choi, Y. *J. Korean Phys. Soc.* **1997**, *30*, S228.

(44) Verdonck, P.; Hasenack, C. M.; Mansano, R. D. *J. Vac. Sci. Technol. B* **1996**, *14* (1), 538.

(45) Tsai, C. J.; Chung, P. L.; Yu, K. H. *Thin Solid Films* **2000**, *365* (1), 72.

(46) The electroless Ni plating bath chosen for this study produces a microcrystalline deposit of 7-nm Ni grains. Initially the EL Ni film is deposited as a coating on individual surface bound colloidal Pd(II) particles, eventually leading to the coalescence of particles and the formation of a continuous film. During the course of our work, AFM and visual examinations of the Ni particulate morphology have indicated no preferred grain orientation for the deposited EL Ni films. Therefore, the grain structure of the EL Ni film is not expected to significantly impact etch selectivity.

(47) Brandow, S. L.; Dressick, W. J.; Dulcey, C. S.; Koloski, T. S.; Shirey, L. M.; Schmidt, J.; Calvert, J. M. *J. Vac. Sci. Technol. B* **1997**, *15* (5), 1818.

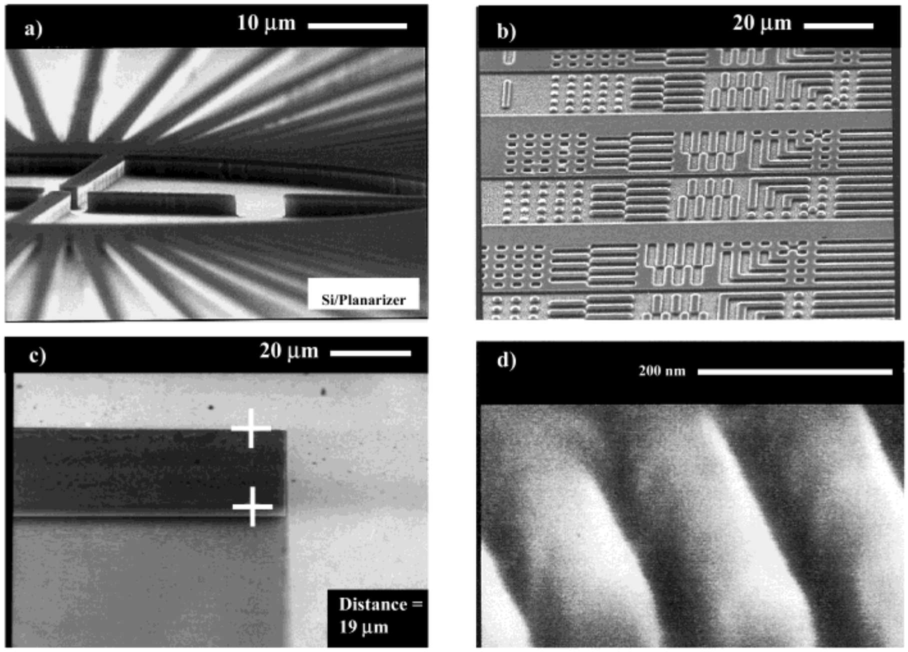

Figure 9. Etched patterns fabricated by (a) DUV photolithography using the CCM process on planarizer, (b) DUV photolithography using the CCM process on a silicon substrate, (c) sidewall profile of a feature etched 19 μm deep into silicon, and (d) high-resolution etched features (~15−24 nm) patterned by STM lithography of a siloxane film. SEM images were taken prior to the removal of the Ni film to avoid surface charging during image acquisition. Etch depths were calibrated to correct for the viewing angle of the SEM and subsequently verified by AFM.

The use of EL Ni etch masks for pattern transfer is particularly attractive as it allows the metallization of nonplanar, insulating substrates using low temperature processes, simple materials, and low-cost equipment. Furthermore, the processing of samples is track-compatible and occurs under ambient, aqueous conditions. The siloxane imaging layers can be engineered to be sensitive to various types of radiation or used in conjunction with standard photoresists in the CCM process. More recently we have extended our method to include the use of physisorbed ligands to create templates for EL Ni deposition,[48,49] as well as the use of new ultrasmall, nearly monodisperse Pd(0) catalyst.[50] The deposited EL Ni exhibits excellent etch resistance while avoiding many of the problems associated with polymeric etch masks such as pattern collapse, outgassing, and postexposure processing constraints. EL metal etch masks have been used to successfully fabricate working CMOS transistors,[7] as templates for contact printing applications,[51] as textured platforms for cell growth,[52] and in the patterning of III−V semiconductor materials.[53,54] Although the etch rate under the conditions used here is relatively slow (~15 nm/min), preliminary experiments indicate that the mask is suitable for inductively coupled plasma (ICP) etching with chlorine species at considerably higher etch rates, making it attractive for MEMS applications.

Acknowledgment. This work was supported by the DARPA Advanced Lithography Program, the DARPA Molecular Level-Printing Program, and the U.S. Naval Research Laboratory Core Research Funding Program, sponsored by the Office of Naval Research.

CM0202308

(48) Dressick, W. J.; Chen, M.-S.; Brandow, S. L. *J. Am. Chem. Soc.* **2000**, *122* (5), 982.
(49) Dressick, W. J.; Nealey, P. F.; Brandow, S. L. *Proc. SPIE* **2001**, *4343*, 294.
(50) Dressick, W. J.; Chen, M.-S.; Brandow, S. L.; Rhee, K. W.; Shirey, L. M.; Perkins, F. K. *Appl. Phys. Lett.* **2001**, *78* (5), 676.
(51) Martin, B. D.; Brandow, S. L.; Dressick, W. J.; Schull, T. L. *Langmuir* **2000**, *16* (25), 9944.
(52) Kapur, R.; Spargo, B. J.; Chen, M.-S.; Calvert, J. M.; Rudolph, A. S. *J. Biomed. Mater. Res.* **1996**, *33* (4), 205.
(53) Shamamian, V.; Dressick, W. J.; Brandow, S. L., unpublished results.
(54) Sheridan, D. C.; Casady, J. B.; Ellis, E. C.; Siergiej, R. R.; Cressler, J. D.; Strong, R. M.; Urban, W. M.; Valek, W. F.; Seiler, C. F.; Buhay, H. *Silicon Carbide Relat. Mater.* **2000**, *338* (3), 1053.